11C.6 ESTIMATING VERTICAL MOTION PROFILE SHAPE WITHIN TROPICAL WEATHER STATES

Zachary J. Handlos * and Larissa E. Back
University of Wisconsin, Madison, Wisconsin

1. INTRODUCTION

Understanding the relationship between tropical convection and the large scale circulation is vital to improving our understanding of weather and climate. At the heart of this relationship is latent heating, both in the horizontal and vertical. Vertical profiles of latent heating (or the distribution of latent heating in the vertical) can provide information about the distribution of where clouds and precipitation develop, as well as provide insight with respect to where atmospheric heating occurs and global energy and moisture budgets.

Unfortunately, vertical latent heating profiles are difficult to retrieve. This is despite the fact that a variety of algorithms have been constructed in order to estimate latent heating profiles and rid of retrieval difficulties. Such difficulties in consistent estimation of latent heating profiles are shown in figure 3 of Hagos et al (2010), where estimated latent heating profiles over the tropical ITCZ (Inter-Tropical Convergence Zone) region vary significantly amongst various estimation algorithms.

Along with latent heating profile retrieval difficulties, the idea that variability of latent heating profiles is associated with percent stratiform rain fraction (Houze 2004) may not necessarily be true in every scenario. For example, Back and Bretherton (2006) (referred throughout this paper as BB06 hereafter) investigate vertical motion profiles (analogous to latent heating profiles) within two regions along the tropical ITCZ (Inter-Tropical Convergence Zone), and this is shown in figure 1. In the western (central-east) Pacific region, a top (bottom) heavy profile is observed, where maximum UVM (upward vertical motion; analogous to a maximum in latent heating) occurs in the upper (lower) troposphere.

Based on Schumacher and Houze (2003), Schumacher et al (2004), Houze (2004) and Jakob and Schumacher (2008), we would expect the western (central-east) Pacific to contain a higher percentage of stratiform (convective) rain fraction. Our figure 1 and table 1 shows that this is not the case, because the percent stratiform rain fraction in the western Pacific, where a top-heavy profile resides, is less than the central-east Pacific, where a bottom-heavy profile resides. Therefore, something else (along with stratiform rain fraction) seems to be associated with vertical motion profile (and thus latent heating profile) variability. A second look at BB06 shows that the magnitude of surface convergence is twice as strong in the central-east Pacific compared to the western Pacific, suggesting that surface convergence is associated with profile variability.

Our work is centered on taking a new approach towards the estimation of latent heating profiles via estimation of vertical motion profiles using observed surface convergence and precipitation data. We first construct two vertical motion basis functions, which describe the most dominant modes of vertical motion profile variability. This is done using a PCA (Principal Component Analysis). After constructing these modes, we constrain our vertical motion profile estimates using the dry static energy budget and mass continuity. From this, we test our methodology by estimating vertical motion profiles for six tropical mesoscale weather states defined in Rossow et al (2005). We test the hypothesis that *latent heating profile shape varies (in space and time) in association with cloud regime type*.

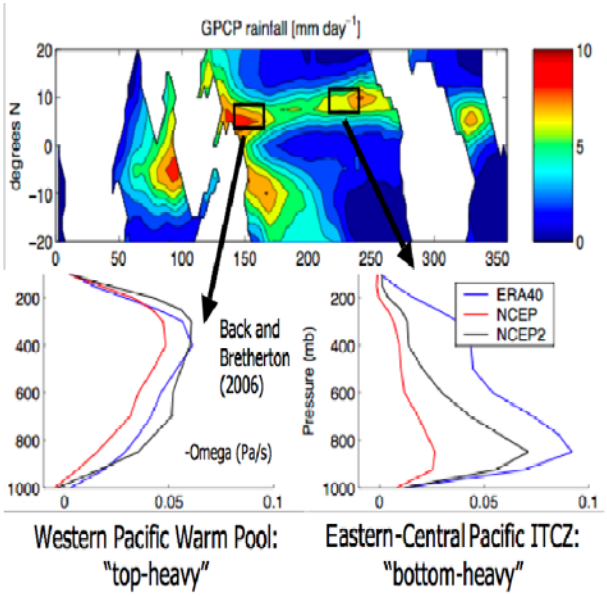

Figure 1: Adapted from BB06, the top panel shows monthly averaged GPCP rainfall in the tropical ITCZ region. The bottom panel plots show reanalysis-estimated vertical motion profiles for the western (left panel) and central-east Pacific (right panel) regions boxed in black in the top panel.

Percent Stratiform Rain Fraction	
Western Pacific	53.56%
Central-East Pacific	58.73%

Table 1: Percent Stratiform Rain Fraction values in regions investigated in BB06 calculated from TRMM algorithm 3A25.

* *Corresponding author address:* Zachary J. Handlos, Univ. of Wisconsin, Dept. of Atmospheric and Oceanic Sciences, 1225 West Dayton Street, Madison, WI 53706; e-mail: handlos@wisc.edu

2. VERTICAL MOTION PROFILES AND LATENT HEATING PROFILES

For this study, we estimate vertical motion profile shape as a proxy for latent heating profile shape. This is because it can be shown in the budget equation for dry static energy with respect to the tropical ITCZ region, assuming steady state and that all precipitation falls out as liquid, that the most dominant terms are the vertical advection of dry static energy and latent heating. This is because horizontal gradients of temperature (and thus dry static energy) are small in the tropics, and because latent heating is the most variable diabatic heating term in this region. From this, since dry static energy approximately increases linearly with height, vertical motion is proportional to latent heating. Hence we can use vertical motion profiles to infer something about the vertical structure of latent heating.

3. RELATIONSHIP BETWEEN VERTICAL MOTION PROFILES, PRECIPITATION, AND SURFACE CONVERGENCE

Figure 2 shows the relationship between ω (vertical motion) profiles, precipitation and surface convergence for a point in the tropical ITCZ region. The left panel shows the effects of precipitation rate given a fixed amount of surface convergence. The blue (red) curve shows a ω-profile in a low (high) precipitation case. It is clear that the area contained within the ω-profile (i.e.: area between ω = 0 and the maximum in negative ω) is greater (less) for the high (low) precipitation case. An increase (decrease) in the area under the ω-profile is proportional to an increase (decrease) in surface precipitation.

The right panel shows the effects of surface convergence for a fixed precipitation rate. The blue (red) curve shows a ω-profile in a low (high) surface convergence scenario. More (less) surface convergence is associated with a more bottom (top) heavy ω-profile.

We use the relationships outlined in figure 2 in estimating ω-profile shape.

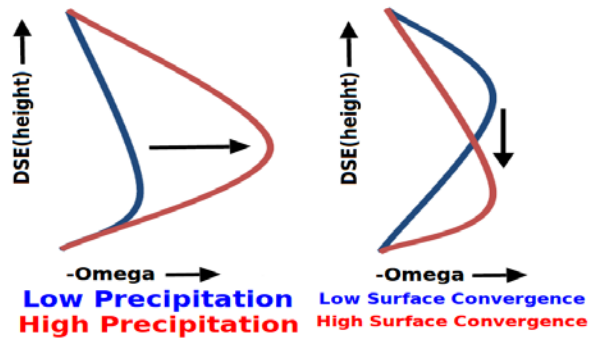

Figure 2: Illustration of the relationship between the shape of the ω-profile and the magnitude of precipitation (left panel), and the relationship between the ω-profile shape and the magnitude of surface convergence (right panel).

4. GENERATING BASIS FUNCTIONS

We assume for our profile estimations that only two dominant modes of ω-profile variability exist in the tropical ITCZ region considered. To estimate these modes, we use PCA on ERA-Interim, NCEP/NCAR (National Centers for Environmental Prediction/National Center for Atmospheric Research) reanalysis, and TOGA-COARE (Tropical Ocean Global Atmosphere Coupled Ocean Atmosphere Response Experiment) data, because we wish to choose basis functions, (or idealized ω-profile shapes) that can describe the maximum amount of variability in the ω-profile. The amount of influence that each basis function has on each space-time grid point we consider is related to the amount of surface convergence and precipitation observed at that point.

Figure 3 shows the two orthogonal (linearly independent) basis functions that are derived from our PCA on each dataset listed above. The ERA Interim (NCEP/NCAR) reanalysis basis functions are shown in blue (black), with the basis functions constructed from the TOGA-COARE dataset shown in red. In all three cases, the first mode (solid curves) shows UVM throughout the middle and upper troposphere, while the second mode (dashed curves) shows maximum UVM near the surface and tropopause. These modes are similar to the vertical motion profile variability shown in the field campaign and reanalysis data in BB06. Note that although these basis functions are derived from reanalysis datasets rather than observations, we use these modes to estimate ω-profiles despite this because we have nothing else to use up to this point.

5. CONSTRAINING VERTICAL MOTION PROFILES

Each estimated ω-profile is a linear combination of basis functions 1 and 2. Since each profile is a linear combination of the two modes of profile variability, our methodology requires calculation of the amplitude of each mode, or the amount of influence that each mode has with respect to the shape of the ω-profile. We determine these amplitudes by constraining ω using precipitation and surface convergence data along with the relationships outlined in figure 2.

Figure 4 compares ERA-Interim reanalysis ω-

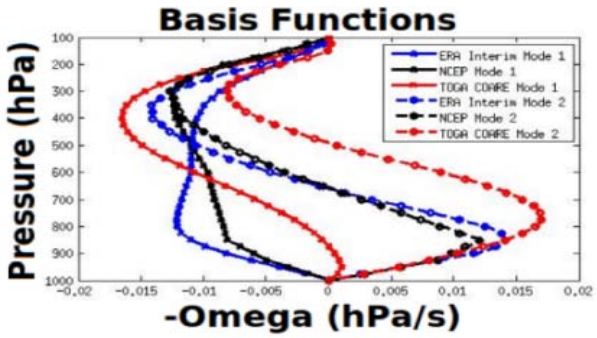

Figure 3: Basis functions constructed from the ERA-Interim (blue) and NCEP/NCAR (black) reanalyses, and the TOGA-COARE (red) dataset.

profiles from the western and central-east Pacific regions investigated in BB06 with ω-profiles that we reconstruct using our methodology. To create this figure, we first use the dry static energy budget and mass continuity to compute precipitation (as a residual) and surface convergence respectively for each region. Then we solve for the amplitudes of each basis function as discussed in the previous paragraph. Finally we linearly combine the two modes of variability to create each ω-profile (solid lines) and compare with the reanalysis ω-profiles (dashed lines).

The figure shows that the system we use to constrain and subsequently reconstruct ω-profiles from ERA-Interim is a closed system. Our reconstructed ω-profiles for the western and central-east Pacific regions investigated in BB06 are nearly identical to the reanalysis ω-profiles from the ERA-Interim dataset. The western (central-east) Pacific reconstructed profile exhibits a top-heavy (bottom-heavy) profile shape, as expected from BB06. The values of surface convergence (which in our study is defined as the slope of the ω-profile curve from 1000 hPa to 975 hPa) are identical in both cases, and the amount of area contained in each profile (for each case) between ω = 0 and the maximum in UVM is very similar. Thus, our system is closed and can be used to estimate ω profiles.

6. RESULTS: ISCCP WEATHER STATE VERTICAL MOTION PROFILES

In order to estimate ω-profiles for the six ISCCP weather states, we used basis functions derived from the ERA-Interim reanalysis datasets along with GPCP (Global Precipitation Climatology Project) one degree daily precipitation, QuikSCAT (Quick Scatterometer) computed surface convergence data, and the ISCCP (International Satellite Cloud Climatology Project) weather states dataset generated via a clustering analysis in Rossow et al (2005). We use the method described in sections 4 and 5. We again assume that there are two dominant modes of ω-profile variability and that ω = 0 at 1000 and 100 hPa. Also, we assume a constant radiational heating value of ~ $-86.81 Wm^{-2}$.

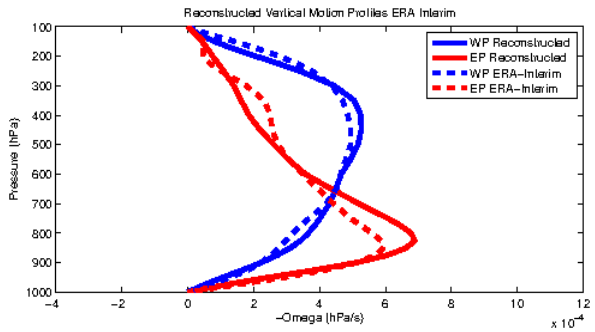

Figure 4: ω-profile shapes generated for the western Pacific (blue) and central-east Pacific (red) regions as defined in BB06 using ERA-Interim (top-left panel) reanalysis data. Solid (dashed) profiles are reconstructed in each region using our methodology (from the reanalysis data itself).

We first estimate ω-profiles for every grid point in the tropical ITCZ region (15ºS to 15ºN latitude; all longitudes) from 2001-2006 using our methodology from the last section. Then, we bin the data into six weather state bins. Finally, the ω-profiles are spatial-temporally averaged in order to generate mean state ω-profiles for each weather state.

The results of this analysis using ERA-Interim data are shown in figure 5. This figure shows that each weather state is associated with a unique ω-profile shape. For example, the vigorous deep convective weather state (solid blue profile in figure 5) exhibits high amounts of precipitation (large area within the curve between ω = 0 and the maximum in UVM ~400 hPa) and strong surface convergence (steep slope in the profile between 975-1000 hPa). The lesser deep convective regime with thick cirrus outflow (solid black profile) exhibits higher amounts of precipitation relative to the other weather states, but has a much smaller magnitude of surface convergence compared to the vigorous deep convection profile. Both the vigorous deep convective and thick cirrus outflow regimes exhibit top-heavy profiles. Both profiles also resemble the top-heavy profile exhibited in the western Pacific reconstructed ω-profile in figure 4.

The isolated convective systems weather state (solid red) is the only convectively active regime from Rossow et al (2005) to exhibit a bottom-heavy profile. This profile has strong surface convergence but lower magnitudes of precipitation compared to the other convectively active regimes. This profile strongly resembles the reconstructed central-east Pacific profile in figure 4.

As for the convectively inactive weather states, the profiles all exhibit surface divergence and minimal precipitation. All of these weather states should not contain high amounts of precipitation on average, and this is confirmed by figure 5.

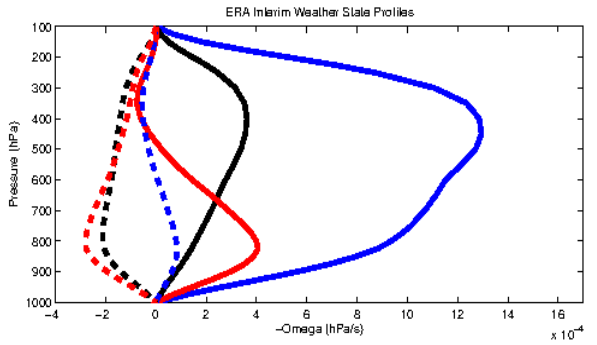

Figure 5: mean state ω-profiles for the six ISCCP weather states defined by Rossow et al (2005) for years 2001-2006. The convectively active (inactive) weather states are vigorous deep convection (thin cirrus) in solid (dashed) blue, lesser deep convection (mixed trade shallow cumulus) with thick cirrus outflow in solid (dashed) black, and isolated, disorganized convective systems (marine stratus) in solid (dashed) red.

Figure 6 shows a method of representing both the amount of variability for the ω-profiles associated with each weather state, as well as the variance of the mean state ω-profiles. The vectors and outer ellipse represent the variability of both the surface convergence and precipitation data for each weather state, as well as the variability of ω-profiles associated with each weather state. The inner ellipses are the confidence intervals (95th percentile with 100 degrees of freedom, a conservative estimate) for the mean state profiles.

This figure was constructed by performing a PCA on combined (and normalized) GPCP precipitation and QuikSCAT surface convergence data. The first (second) EOF (Empirical Orthogonal Function) is represented as a vector directed in the positive (negative) surface convergence and positive precipitation directions in figure 6 for each weather state. The first (second) EOF represents the variability with respect to the surface convergence and precipitation data itself (variability with respect to the data as well as the shape of the ω-profile). The outer ellipse (bold ellipse), with major (minor) axis equal to the magnitude of EOF 1 (EOF 2), represents the range of variability associated with the ω-profiles associated with each weather state. The center of each ellipse represents the mean surface convergence and precipitation associated with each mean state ω-profile.

Figure 6 shows that the mean state ω-profile shapes for each weather state are well constrained. Therefore, the mean state profiles associated with each weather state are unique. On the other hand, each weather state exhibits significant variability with respect to the various ω-profile shapes associated with each weather state. Thus, if one were to estimate the shape of a ω-profile at a grid point, it may be difficult to determine which weather state is associated with this particular profile. When investigating the mean state of the tropical ITCZ, one would be able to identify the weather state that matches the estimated profile shape.

7. CONCLUSIONS

The goal of this study was to test the hypothesis that latent heating profile shape varies (in space and time) in association with cloud regime type. We do this by estimating ω-profiles for six ISCCP mesoscale tropical weather states (Rossow et al 2005). We apply an innovative methodology that estimates ω-profiles using observed precipitation and surface convergence data.

We showed that ω-profile variability (analogous to latent heating profile variability) is not solely associated with stratiform rain fraction, but is also associated with the magnitude of surface convergence at the point of interest (figure 1). We also showed that each weather state is associated with its own unique mean state ω-profile (figure 5). Finally, while the mean ω-profile shapes are well constrained, the amount of ω-profile variability with respect to each weather states is observed to be large in our work (figure 6).

8. REFERENCES

Back, L. E., and C. S. Bretherton, 2006: Geographic variability in the export of moist static energy and vertical motion profiles in the tropical Pacific Geophys. Res. Lett., 33, L17810, doi:10.1029/2006GL026672.

Hagos, Samson, and Coauthors, 2010: Estimates of Tropical Diabatic Heating Profiles: Commonalities and Uncertainties. *J. Climate*, **23**, 542–558. doi: http://dx.doi.org/10.1175/2009JCLI3025.1

Houze, R. A., Jr., 2004: Mesoscale convective systems. Rev. Geophys., 42, 10.1029/2004RG000150, 43 pp.

Jakob, C., and C. Schumacher, 2008: Precipitation and latent heating characteristics of the major Tropical Western Pacific cloud regimes. J. Climate, 21, 4348-4364.

Rossow, W.B., G. Tselioudis, A. Polak, and C. Jakob, 2005: Tropical climate described as a distribution of weather states indicated by distinct mesoscale cloud property mixtures. Geophys. Res. Lett., 32, L21812, doi:10.1029/2005GL024584.

Schumacher, Courtney, Robert A. Houze, Ian Kraucunas, 2004: The Tropical Dynamical Response to Latent Heating Estimates Derived from the TRMM Precipitation Radar. J. Atmos. Sci., 61, 1341–1358. doi:10.1175/15200469(2004)061<1341:TTDRTL>2.0.CO;2

Schumacher, C., and R. A. Houze Jr., 2003: Stratiform rain in the tropics as seen by the TRMM Precipitation Radar. J. Climate, 16, 1739-1756.

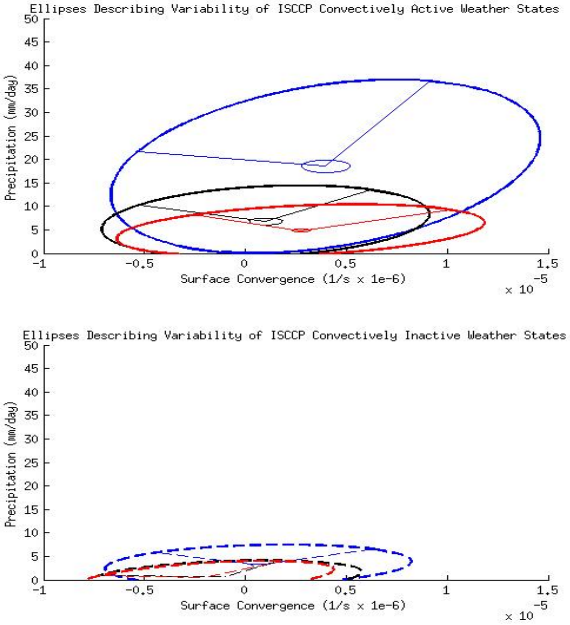

Figure 6: Ellipses representing variability (outer), confidence intervals (inner) associated with the convectively active (inactive) weather states (same color and line scheme for each weather state as in figure 5).